2012

Resonant Inelastic X-ray Scattering of Methyl Chloride at the Chlorine K Edge

L. El Khoury
University of Paris

Loic Journel
University of Paris

Renaud Guillemin
University of Paris, renaud.guillemin@upmc.fr

Stephane Carniato
University of Paris

Wayne C. Stolte
University of Nevada, Las Vegas, wcstolte@lbl.gov

Resonant inelastic x-ray scattering of methyl chloride at the chlorine K edge

L. El Khoury,[1,2] L. Journel,[1,2,a)] R. Guillemin,[1,2] S. Carniato,[1,2] W. C. Stolte,[3,4,5] T. Marin,[1,2] D. W. Lindle,[3,4] and M. Simon[1,2]
[1]*UPMC Univ Paris 06, UMR7614, Laboratoire de Chimie Physique-Matière et Rayonnement, F-7005 Paris, France*
[2]*CNRS, LCPMR(UMR 7614), 11 rue Pierre et Marie Curie, 75231 Parix Cedex 05, France*
[3]*Advanced Light Source, Lawrence Berkeley National Laboratory, Berkeley, California 94720, USA*
[4]*Department of Chemistry, University of Nevada, Las Vegas, Nevada 89154-4009, USA*
[5]*Harry Reid Center for Environmental Studies, University of Nevada, Las Vegas, Nevada 89154-4003, USA*

(Received 4 October 2011; accepted 18 December 2011; published online 12 January 2012)

We present a combined experimental and theoretical study of isolated CH_3Cl molecules using resonant inelastic x-ray scattering (RIXS). The high-resolution spectra allow extraction of information about nuclear dynamics in the core-excited molecule. Polarization-resolved RIXS spectra exhibit linear dichroism in the spin-orbit intensities, a result interpreted as due to chemical environment and singlet-triplet exchange in the molecular core levels. From analysis of the polarization-resolved data, Cl $2p_{x,y}$ and $2p_z$ electronic populations can be determined. © *2012 American Institute of Physics*. [doi:10.1063/1.3675685]

I. INTRODUCTION

Methyl chloride is the most abundant organohalogen anthropogenic or natural in the atmosphere. A large amount of methyl chloride is produced naturally in the oceans by the action of sunlight on biomass[1] or artificially by reaction of chloride acids on methanol. Considerable study has been made of the photodissociation dynamics of CH_3Cl in the UV range due to its role as a source of atomic Cl.[2–6]

In contrast, very few results on this molecule have been published using x-ray spectroscopy, where deep-inner electrons can interact with x-rays. We note, in particular, a study done using coincidence techniques,[7] showing fast dissociation of the molecule after resonant Cl 1*s* photoexcitation into the lowest unoccupied molecular orbital (LUMO), $8a_1$. Mass spectra recorded with respect to the incident polarization vector were used to confirm the symmetry of the $8a_1$ antibonding LUMO. Several other studies have shown[8–10] fast fragmentation of the molecule after core excitation near the Cl $L_{2,3}$ edge, leading to the formation of either Cl^+ or HCl^+. The Auger–Doppler shift also has been observed for various orientations of the electron and fragment ion.[9] Partial-ion-yield experiments on CH_3Cl excited in the vicinity of the Cl 2*p* inner shell have shown site-selective fragmentation along the C–Cl bond axis and strong intensity dependence of Rydberg transitions on fragment size.[7,10]

Resonant inelastic x-ray scattering (RIXS), on the other hand, is a powerful tool for elucidating the electronic properties of gas-phase molecules. The physical process underlying RIXS corresponds to resonant excitation of an inner-shell electron followed by relaxation of the core-hole via radiative decay, i.e., x-ray photon emission. For example, RIXS properties have been used to disentangle different two-electron atomic processes (shake-off, shake-up, resonant double excitations) in the vicinity of an inner-shell threshold in Argon atoms.[11] RIXS also was used to study the energy dependence of K+L double photoexcitation satellites[12] from threshold to saturation. Their probabilities were deduced from satellite-to-diagram line yield ratios I(KL-$L_{2,3L}$):I(K-$L_{2,3L}$).

This technique also has been shown to be extremely sensitive to molecular dynamics initiated by resonant inner-shell photoexcitation. As recently demonstrated in free HCl molecules, the lifetime of the core-excited state can be used to probe the nuclear motion and give indirect access to time-resolved spectroscopy in the sub-femtosecond domain.[13,14] Furthermore, measuring the K_α emission lines (also known as KL transition, we use here the historical notation K_α) for different angles θ between the incident polarization and the outgoing polarization, linear dichroism has been observed in several molecules. Variations of the spin-orbit ratio ($2p_{3/2}$:$2p_{1/2}$) with θ, observed in both HCl and CF_3Cl, have been interpreted as due to molecular field effects, including singlet-triplet exchange,[15,16] affecting the molecular core-levels. The influence of molecular-field effects and the influence of p_x, p_y, and p_z orbitals on the 2*p* core-hole states was first evidenced in photoelectron and Auger electron spectroscopy.[17–19] Polarized RIXS on HCl and CF_3Cl was shown to provide direct measurement of the electronic populations in the $p_{x,y,z}$ components.

In this article, we report a study combining experimental high-resolution RIXS measurements and theoretical calculations on isolated CH_3Cl molecules after Cl K photoexcitation. Section II describes the different experimental setups used in this study. The theoretical framework used for the calculations is detailed in Sec. III. Absorption and molecular features in high-resolution RIXS are illustrated in Sec. IV A; angular and polarization properties are discussed in Sec. IV B. Finally, we provide conclusions in Sec. IV.

a)Author to whom correspondence should be addressed. Electronic mail: loic.journel@upmc.fr.

II. EXPERIMENTAL DETAILS

Two different experimental setups were used to record the experimental data presented in this article. The first one is dedicated to measurements of high-resolution RIXS spectra in gas-phase samples and has been described in detail previously.[20] Briefly, it consists of a bent-crystal Rowland-circle spectrometer based on the Johann geometry. The intense photon beam (400 meV bandwidth at the Cl K edge, horizontally polarized) delivered by the LUCIA undulator[21] beamline at the SLS electron storage ring (Swiss Light Source, PSI, Villigen, Switzerland) is focused into a gas cell containing ~300 mbar of methyl chloride. The scattering plane is horizontal, and the scattered photons are energy analyzed in a vertical plane at 45° from the incident beam direction by a $(11\bar{2}0)$ quartz crystal. This crystal reflects and focuses the scattered beam onto a gas proportional counter. At the energy of the Cl K_α lines (2620 eV), the crystal has a Bragg angle of ~74°. This leads to an experimental resolution of 360 meV[20] for the spectrometer, highest resolution ever achieved in this energy range. A Si photodiode was placed behind the gas cell to record absorption spectra.

Measurements of the polarization properties of the x-ray emission after core photoexcitation were performed on the x-ray spectrometer at beamline 9.3.1 of the Advanced Light Source (ALS, Berkeley, USA).[22] Briefly, it consists of a crystal Rowland-circle spectrometer. The 9.3.1 beamline provides an intense photon beam ~100% linearly polarized in the horizontal plane, focused into a gas cell containing up to 400 mbar of methyl chloride. The scattering plane is vertical and the scattered beam is energy-analyzed and focused onto a position sensitive detector by a Si(111) crystal, yielding an energy resolution of 400 meV. At the energy of the Cl K_α lines, the Bragg angle is 49°, very close to the x-ray Brewster angle 45°, where reflectivity of the π-component of the polarization approaches zero; less than 2% of the π-contribution is expected at 2620 eV for the chlorine K_α emission lines.[23] Thus, only σ-polarized waves are diffracted efficiently and the reflected beam is nearly fully σ-polarized. Under these conditions, the crystal acts as both an energy analyzer and a polarimeter. By rotating the spectrometer around the vertical axis passing through the center of the gas cell and the crystal, we are able to analyze the polarization ($\vec{e}_2$) of the scattered light for different angles with respect to the incident polarization ($\vec{e}_1$), thus performing polarization-resolved-RIXS.[15,16]

III. THEORETICAL DETAILS

Methyl chloride molecule is a closed-shell molecule with 26 electrons. The ground state electronic configuration belongs to the C_{3v} point group and can be written as

$$(1a_1)^2(2a_1)^2(3a_1)^2(4a_1)^2(1e)^4$$
$$(5a_1)^2(6a_1)^2(2e)^4(7a_1)^2(3e)^4(8a_1)^0,$$

where the first five (atomic-like) orbitals correspond to the inner-shell orbitals with 1*s*, 2*s*, or 2*p* character localized on the Cl and C atoms. The $5a_1$ and $6a_1$ orbitals correspond to inner-valence-shell states, whereas the $2e$, $7a_1$, and $3e$ are the outer-valence-shell molecular orbitals. The $8a_1$ orbital is the lowest unoccupied molecular orbital (LUMO).

After resonant excitation of a Cl 1*s* core electron, radiative K_α emission is a spectator decay which leaves the molecule in the $2p^{-1}8a_1^1$ core-excited state. In the case of 2*p* core ionization, the relativistic wave function is built on non-relativistic doublet states separated in energy by the combined influences of the molecular field and spin-orbit (SO) splittings. In the case of core excitation resulting in a 2*p* hole, the energetic structure of the final $2p^{-1}$ core-excited states is mainly determined by the SO splitting of the core shell, the molecular field, and the singlet-triplet exchange energy. Due to SO interaction, the relativistic wave functions are a strong mixture of singlet and triplet states.

The low-lying $2p^{-1}8a_1^1$ SO components, including non-relativistic states for CH_3Cl at the bond length used in the calculations ($R_0 = 1.798\,\text{Å}$, close to the accepted experimental value $R_{eq} = 1.776\,\text{Å}$ value[24]), were determined *ab initio*. The full Breit–Pauli coupling[25–27] integral package in GAMESS (US),[28] including the SO interaction, was used for calculations of the $(2p^{-1})$ core-excited states. SO-coupling calculations were performed on variational configuration-interaction (CI) wavefunctions dubbed SO-CI. In such a procedure, a model Hamiltonian in the complete active-space configuration-interaction (CAS-CI) basis is built and diagonalized to produce spin-mixed states, which are linear combinations of the complete active-space CI states. The Hamiltonian matrix is a sum of spin-free terms and spin-orbit terms $H = H_{sf} + H_{so}$. For SO-CI, the matrix H_{sf} is diagonal in the CAS-CI state basis, with the LS-coupled CAS-CI energies as the diagonal elements, and H_{so} contains only off-diagonal couplings between these LS states. The CI active space includes the three occupied $2p_{x,y,z}$ inner shells and the 80 lowest-unoccupied virtual orbitals, all derived from the non-relativistic $2s^{-1}8a_1^1$ potential. The core-excited reference wavefunction was represented by a generalized $2s^{-1}8a_1^1$ singlet state to avoid orientational effects artificially induced in the calculations using $2p_{x,y,z}^{-1}8a_1^1$ states. Because the 2*s* and 2*p* orbitals are close in energy ($\Delta E \sim 70$ eV),[10] similar relaxation effects are expected.

In order to determine Franck–Condon factors, we calculated the change in normal coordinates for the following transitions: (i) the neutral ground state to the 1*s* core-excited state; and (ii) the 1*s* core-excited state to the 2*p* core-excited state. In principle, for path (i), direct calculations of Franck–Condon factors face the difficulty that stretching of the C–Cl bond in the dissociative $(1s)^{-1}$ core-excited state can be accompanied by deformation of the CH_3 radical. Thanks to the present calculations, we have shown that deformations of the C–H bond length (less than ~0.01 Å) and H–C–H angle (~2°) in CH_3 remain small in the Franck–Condon region (1.65 Å$<R_o<$1.92 Å). In addition, because H–Cl bond elongation for HCl is only 0.1 *Å* within the core-hole lifetime (≈1 fs), a shorter bond elongation is expected in the case of higher-mass CH_3Cl molecule. Consequently, we neglect CH_3 umbrella deformation and adopt a one-dimensional approximation, along the C–Cl bond, for the dissociative state.

All of the relevant potential-energy surfaces (PES) were calculated *ab initio*. The dissociative Cl $(1s)^{-1}$

core-excited PES for CH_3Cl has been computed at the density functional theory (DFT) level, with the Kohn–Sham scheme using a hybrid B3LYP correlation-exchange functional. The application of DFT to core-excitation phenomena takes advantage of the fact that both relaxation and correlation effects are described simultaneously at a moderate computational cost compared to self-consistent field and post-Hartree–Fock methods. For singlet core-excited-state calculations, a local modified version of GAMESS was used. The excitation energies of the core-excited singlet states are calculated using the Kohn–Sham approach in combination with the sum method of Ziegler *et al.*[29] The DFT calculations were performed at different representative C–Cl interatomic distances, ranging from 1.1 to 6.0 Å. The nuclear wavefunctions for the dissociative states were calculated using a one-dimensional Hamiltonian model that can be written as

$$H = -\frac{\hbar^2}{2\mu}\frac{d^2}{dr^2} + V(R_{C-Cl}),$$

where μ is the reduced mass of the system and $V(R_{C-Cl})$ is the vibrational potential along the C–Cl bond. The eigenvectors and eigenvalues were obtained by diagonalizing the Hamiltonian using the finite-difference approximation.[30] In the present case, because the holes in the $1s$ and $2p$ levels are very similar from the point of view of a chemical bond, we assumed that the $1s$ core-hole intermediate PES and the final $2p$-hole PES are parallel.[13]

All calculations were performed using a large flexible basis set (aug/cc/pCVQZ)[31] for Cl to describe electronic relaxation, correlations, and SO coupling in inner-shell core-excited states. With the basis sets, the carbon and hydrogen atoms were described by a 6-311 G polarized basis set with a $(4s, 3p)$ contraction.[32]

IV. K_α EMISSION LINES IN METHYL CHLORIDE

A. K_α molecular features: dynamical effects

Figure 1 presents a recorded absorption spectrum measured at the SLS facility in the 2820−2830 eV incident photon-energy range around the Cl K edge. This spectrum

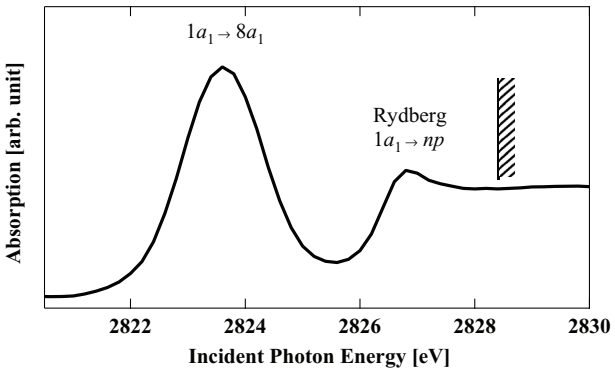

FIG. 1. X-ray absorption spectrum around the Cl K edge of methyl chloride. The first resonance at 2823.5 eV corresponds to the promotion of a $1a_1$ core electron to the $8a_1$ LUMO. This resonance is dissociative. The second resonance corresponds to overlapping excitations to np Rydberg states. The threshold at 2828.4 eV is indicated by the vertical bar.

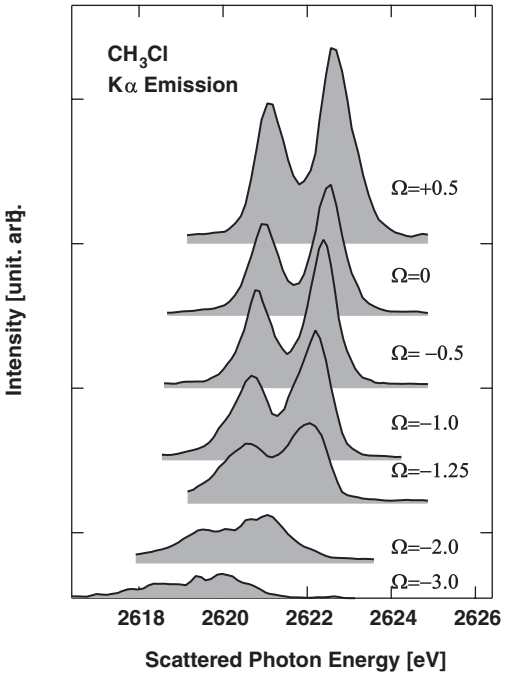

FIG. 2. $K_{\alpha 1,2}$ emission lines as a function of the excitation energy (given by Ω in eV) around the Cl $1s \rightarrow 8a_1$ dissociative resonance.

was recorded in transmission mode using the silicon photodiode placed behind the gas cell to monitor the transmitted photon beam, after proper normalization to the incident beam intensity.

The broad peak at 2823.5 eV corresponds to the transition of a Cl $1s$ electron into the antibonding LUMO, leaving the molecule in a dissociative state.[33] The second maximum at 2826.7 eV is attributed to transitions to Rydberg states of $(1a_1 \rightarrow np)$ symmetry converging to the threshold at 2828.4 eV, indicated by the vertical bar in Fig. 1.

K_α RIXS spectra corresponding to Cl $1s^{-1} \rightarrow 2p^{-1}$ (CH_3Cl $1a_1^{-1} \rightarrow 4a_1^{-1}$ or $1e^{-1}$) transitions where a Cl $2p$ electron fills a $1s$-hole after photoexcitation to the first dissociative state are shown in Fig. 2. The measurement was done using the high-resolution spectrometer described above with a total experimental resolution of 540 meV.[20] The relative scattered intensity is plotted against emitted photon energy for various excitation photon energies, where $\Omega = \omega - \omega_0$ is the energy detuning between the incident photon energy ω and the energy at the top of the Cl $1s \rightarrow 8a_1$ resonance ($\omega_0 = 2823.5$ eV). In Fig. 2, we observe a clear dependence of both the spectral shape and the position of the K_α emission lines on the incident photon energy Ω over the Cl $1s \rightarrow 8a_1$ resonance.

The Ω dependence of the full width at half maximum (FWHM) and the energy position of the K_α lines were monitored across the Cl $1s \rightarrow 8a_1$ resonance. The K_α emission lines were fitted using Voigt profiles assuming two SO components. The FWHM is deduced directly from the width of the Voigt profile and includes the $1s/2p$-core-hole lifetime broadening ($\Gamma_{1s} \sim 0.64$ eV,[34] $\Gamma_{2p} \sim 0.085$ eV,[35]), the experimental broadening ($\Gamma_{Spectro.} \sim 0.36$ eV), and the incident photon bandwidth (~0.4 eV[20]). For large positive detuning ($\Omega > 0$), the emission lines cannot be fitted well by only two Voigt

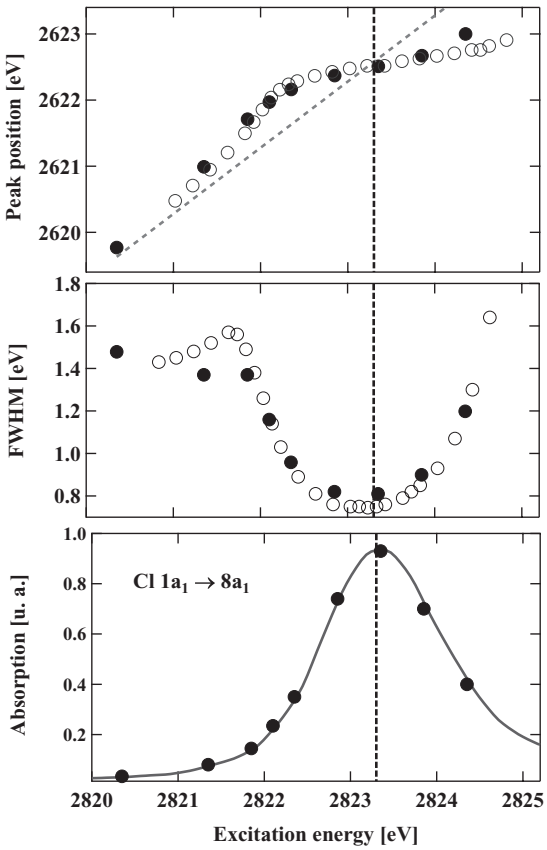

FIG. 3. Top panel: Position of the $K_{\alpha 1}$ emission line for different excitation energies as indicated on the absorption spectrum of the bottom panel with respect to the maximum of the resonance at 2823.25 eV. Full circles are the experimental data, open circles results of the theoretical calculations. Middle panel: Width of the $K_{\alpha 1}$ emission line for the same excitation energies.

profiles because of the presence of Rydberg excitations lying a few eV above the first resonance leading to additional emission lines. Coherent excitation to the $1s^{-1}6\sigma^*$ and Rydberg states leads to interferences that also complicate the emission profile.[36]

The results are summarized in Fig. 3. The lower panel shows the absorption intensity at the first $1s \rightarrow 8a_1$ resonance. The circles indicate photon energies at which emission spectra were recorded (see Fig. 2). The middle panel shows the experimental FWHM (full circles) obtained from the fit to the $K_{\alpha 1}$ lines, corresponding to the $1s2p_{3/2}$ transition, for different excitation energies around the resonance, together with theoretical widths (open circles) obtained from the DFT calculation. Both K_α lines show the same behavior in term of dispersion and FWHM, so only results for the $K_{\alpha 1}$ line are presented and discussed here. On top of the resonance ($\Omega \sim 0$), the K_α emission lines are well resolved and exhibit the characteristic spin-orbit doublet with an energy separation of $\approx$1.60 eV, whereas for large energy detuning, we observe broadening of the two lines. The FWHM exhibits a significant narrowing from $\sim$1.4 eV for excitation energies below resonance ($\Omega < 0$) to $\sim 0.8\,eV$ at $\Omega = 0$ (2823.5 eV), approaching the natural width $\Gamma_{1s} \sim 0.64$ eV). For positive energy detuning ($\Omega > 0$), the FWHM increases off-resonance, as expected. The top panel of Fig. 3 shows the position of the $K_{\alpha 1}$ line across the resonance. Full circles are the experimental data, and the open ones are from the calculations. For excitation energies far below resonance, we observe linear dispersion of the $K_{\alpha 1}$ line position with excitation energy as expected from energy conservation for a Raman process. Through the resonance, we see a transition from linear dispersion to non-dispersive behavior. Linear dispersion is gradually restored when the excitation energy is again tuned away from the resonance.

Following the Kramers–Heisenberg description of the double differential RIXS cross section $\sigma_0(\omega, \omega_1)$[37–40] for an initial state $|i\rangle$ absorbing a photon of energy ω to a core-excited intermediate state $|c\rangle$ which decays by emitting an x-ray photon of energy ω_1 to a final state $|f\rangle$, the transition matrix elements are given by

$$F = \sum_c \frac{\langle f|\widehat{D}|c\rangle\langle c|\widehat{D}|i\rangle}{E - \omega_{cf} + i\Gamma_{1s}}, \tag{1}$$

where $\omega_{cf} = E_c - E_f$ is the energy of the transition between the intermediate (energy E_c) and final states (E_f), Γ_{1s} is the lifetime broadening of the core-excited intermediate state, and $\widehat{D}$ are dipole operators representing the interaction of the target with the x-ray photons.

In this case, where PES of the $1s^{-1}$ intermediate state and the $2p^{-1}$ final state are parallel, the matrix elements can be simplified and the Franck–Condon (FC) factors between parallel PES reduce to a Dirac function. The RIXS cross section $\sigma_0(\omega, \omega_1)$ takes the simple form of a product of an exponential (bound-free FC factor between initial state and dissociative state) and a Lorentzian function accounting for the lifetime Γ_{1s} of the core-hole final state,

$$\sigma_0(\omega, \omega_1) \propto \frac{exp(-[(\omega_1 - \omega)/\Delta]^2 2\ln 2)}{(\omega_1 - \omega_{cf})^2 + (\Gamma_{1s}/2)^2}, \tag{2}$$

where $\Delta = 1.3$ eV is the FWHM of the FC factor determined from *ab initio* DFT calculations (see Sec. III). For comparison with the experimental data, the emission profile described in Eq. (2) is convoluted with a Gaussian instrumental function, taking into account the spectral resolution of the incoming photon beam and the spectrometer resolution, assuming a total experimental resolution of 540 meV.[20] This profile should properly describe Cl K_α emission in CH_3Cl, if the dissociative potential energy surfaces of the intermediate and final states are nearly parallel (see Sec. III).

From Eq. (2), it is apparent that RIXS spectral features are affected by the molecular resonance[41] if $\Gamma/\Delta < 1$. In CH_3Cl, the width of the vibrational broadening ($\Delta = 1.3$ eV) is larger than the width of the natural lifetime broadening of the $1s$ core hole, $\Gamma_{1s} = 0.64$ eV yielding $\Gamma/\Delta \sim 0.5$. Depending on the relative values of Ω, Γ_{1s}, and Δ, the profile of the emission lines is controlled by the product in Eq. (2), and one can distinguish between different regimes. Away from the resonance, i.e., for large detuning, the lineshape of K_α emission is dominated by the FC distribution, described by a Gaussian function, and its dispersion is linear with photon energy. Across the resonance, the line shape is strongly affected by the quenching of the vibrational broadening as the line width approaches Γ_{1s}. The results

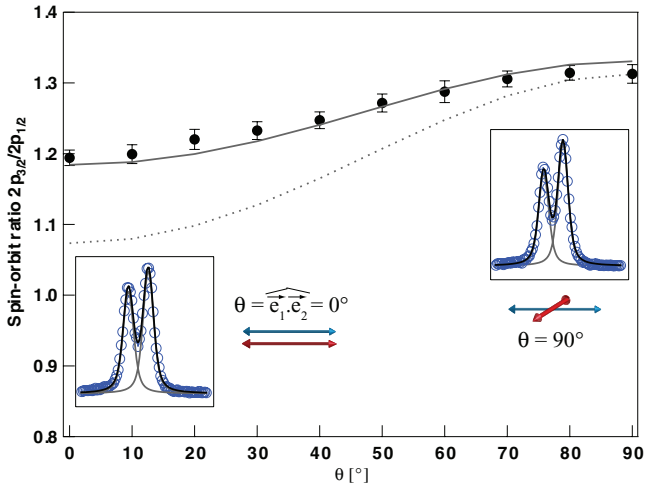

FIG. 4. Ratio of the SO doublet $2p_{3/2}/2p_{1/2}$ as a function of θ. The solid curve is a fit to the experimental data following Eq. (3). The dashed curve is from an *ab initio* CI-SO calculation. The insets show K_α lines fitted by two Voigt functions for two different relative angles between incident and scattered polarizations: 0° and 90°.

observed here in CH_3Cl at high resolution, i.e., dispersive/non-dispersive behavior and broadening/narrowing of the K_α lines depending on the detuning, are similar to those already observed in HCl[13] and DCl,[14] confirming the general character of these features in molecular RIXS.

B. Linear dichroism in the polarization dependence of K_α emission

Polarized x-ray emission is a technique sensitive to molecular orientation and the geometry of orbitals. It has been shown that polarized x-ray-emission spectroscopy allows direct determination of the symmetries of occupied/unoccupied valence molecular orbitals and the anisotropy in absorption and emission processes.[33,42–44]

Using the polarimeter capabilities of the ALS spectrometer, K_α emission lines were recorded after resonant photoexcitation at the Cl $1s \rightarrow 8a_1$ resonance for ten different θ angles between incident ($\vec{e}_1$) and emitted ($\vec{e}_2$) polarization vectors. The experimental spin-orbit ratio were measured from a least-squares fit procedure of the K_α emission lines by two Voigt profiles assuming identical emission profiles for the SO doublet $2p_{3/2}$ and $2p_{1/2}$.

Figure 4 shows the experimental $2p_{3/2}$: $2p_{1/2}$ SO ratio (full circles) for ten different values of θ. This ratio differs strongly from the statistical population ratio 2:1 expected in the atomic case.

Theoretical analysis[16] shows that proper decomposition of the $2p^{-1}8a_1$ final states can be made by six subcomponents including $2p_x^{-1}$, $2p_y^{-1}$, and $2p_z^{-1}$ for each SO component. However, the $2p_x^{-1}$ and $2p_y^{-1}$ states are degenerate, so it is sufficient to fit each ($2p_{3/2}$ and $2p_{1/2}$) SO-component with only two subcomponents, following the procedure previously used for HCl and CF_3Cl.[15,16]

For randomly oriented molecules, the mean-squared scattering amplitude has to be averaged over all spatial

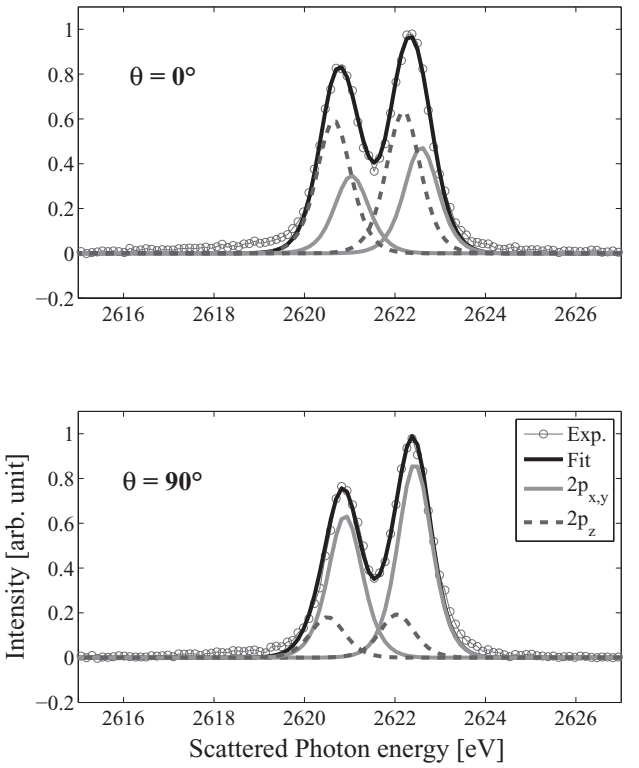

FIG. 5. Experimental K_α emission spectra (circles) obtained at $\theta = 0°$ and 90° between the incident and scattered x-ray polarization vectors for CH_3Cl. Solid black curves are fits to the spectra. For each spin-orbit component, two non-degenerate sublevels, $2p_z$ (dashed gray curves) and $2p_{x(y)}$ (solid gray curves), are included.

orientations[45] and can be written as

$$\langle |F_{2p\,8a_1}|^2 \rangle = 2(1+2\cos^2\theta)\left[F^{zz}_{2p_z 8a_1} F^{zz*}_{2p_z 8a_1}\right] W_S^z + 4(2-\cos^2\theta)\left[F^{x(y)z}_{2p_{x(y)}8a_1} F^{x(y)z*}_{2p_{x(y)}8a_1}\right] W_S^{x(y)}. \quad (3)$$

This formula explicitly includes polarization dependence for the $2p_{x(y)}^{-1}$ and $2p_z^{-1}$ components. W_S^z and $W_S^{x(y)}$ are singlet populations of $2p_z^{-1}8a_1^{+1}$ and $2p_{x(y)}^{-1}8a_1^{+1}$ because only singlet sub-levels contribute to the relativistic $2p^{-1}8a_1^{+1}$ state due to selection rules. The profile of each subcomponent has been determined theoretically assuming parallel potential energy surfaces for the $1s^{-1}8a_1^{+1}$ and $2p^{-1}8a_1^{+1}$ states. The spectra were fitted simultaneously for the ten spectra (θ values ranging from 0 to 90°) using these profiles to represent the four components assuming same energy width for the four components which was fixed in the fitting procedure. Relative intensities were kept as free parameters. The spin-orbit splitting as well as the energy splitting between $2p_z$ and $2p_{x,y}$ for all ten spectra were varied in the procedure. The results are shown in Fig. 5 for $\theta = 0$ and 90°, where experimental data (circles) are plotted together with the fits (solid black curves) to 4 subcomponents ($2p_z$, gray dashed curves, and $2p_{x,y}$, gray solid curves). For CH_3Cl, we find from the fitting procedure that $2p_z$ contributes 52.0(5)% to $2p_{3/2}$ and 48.0(5)% to $2p_{1/2}$ ($2p_{x,y}$ contributes 57.0(5)% and 43.0(5)%, respectively). The energy splitting between $2p_{x,y}$ and $2p_z$ is found to be 0.38 eV.

TABLE I. Population (%) of the spin-orbit subcomponents determined experimentally from the fit of K_α emission lines and theoretically from a SO-CI calculation.

	Exp.		SO-CI	
	$2p_{3/2}$	$2p_{1/2}$	$2p_{3/2}$	$2p_{1/2}$
$2p_{x,y}\,(^1E)$	57.0(5)	43.0(5)	58	42
$2p_z\,(^1A_1)$	52.0(5)	48.0(5)	48	52

The solid curve in Fig. 4 results from a fit to the data using Eq. (3), giving a weight of 58% to the $2p_{x,y}\,(^1E)$ in the $2p_{3/2}$ component and a contribution of 52% in the $2p_z\,(^1A_1)$ sub-component to the $2p_{3/2}$, in excellent agreement with the populations determined from the fit of the ten K_α spectra. The dash curve is from *ab initio* calculations using the SO-CI method and leads to contributions of 58% ($2p_{x,y}(^1E)$ in $2p_{3/2}$) and 48%($2p_z(^1A_1)$ in $2p_{3/2}$).

Equation (3) indicates that the method is highly sensitive to the electronic state populations. A variation of 1% in the population translates into a variation of 3% to 4% in the spin-orbit ratio. In our measurements, experimental uncertainties on the determination of the spin-orbit ratios amount to a 0.5% error on the populations. The deviation between the Bragg angle (49°) and the Brewster angle (45°) adds a systematic error of 0.4% due to imperfect polarization. Although a discrepancy can be observed in Fig. 4 between the two curves, specially at 0°, the derived electronic states populations by full CI-SO calculations and the experimental data: 57% vs 58% for the $2p_{x,y}$ populations and 48% vs 52% on the $2p_z$ populations are in fairly good agreement. The explanation is quite simple. According to Eq. (3), at 90°, the spin-orbit ratio is mainly dominated by the $2p_{x(y)}$ contribution, for which the $2p_{x(y)}$ population values extracted by theory and experiment are in excellent agreement. In contrast, at 0°, there is a contribution of both $2p_z$ and $2p_{x(y)}$ sub-components while a slight larger discrepancy (∼8%) between theory and experiment is observed for $2p_z$ populations. In spite the small difference between theoretical (48%) and experimental (52%) values, we would like emphasize that the general shape as a function of θ is well reproduced by the full SO-CI *ab initio* calculations, as it was already the cases for HCl and CF_3Cl compounds.[15,16] Experimental and theoretical populations are given in Table I.

Table II summarizes the results obtained for different chlorinated compounds. In the table are reported the populations of $2p_{x,y}^{-1}6\sigma^{*+1}$ and $2p_z^{-1}6\sigma^{*+1}$ states in the $2p_{3/2}$ SO component for CH_3Cl, HCl, and CF_3Cl, showing the sensitivity of polarized RIXS to the chemical environment introduced by the different moieties bonded to the chlorine atom. Because of the small number of chlorinated compounds studied to date, it is premature to identify a general trend linking the $2p_{x,y}^{-1}6\sigma^{*+1}$ and $2p_z^{-1}6\sigma^{*+1}$ populations to properties of the constituents. Nonetheless, the results demonstrate that polarized-RIXS experiments allow unequivocal determination of SO-component populations and provide a sensitive probe of molecular-field effects on electronic structure.

TABLE II. $2p_z$ population (%) of the $2p_{3/2}$ spin-orbit component as determined experimentally for CH_3Cl (this study), HCl,[15,16] and CF_3Cl.[15,16]

	CH_3Cl	HCl	CF_3Cl
$2p_{x,y}$	57.0(5)	59.0(5)	60.0(5)
$2p_z$	52.0(5)	54.0(5)	46.5(5)

V. CONCLUSION

We have performed a resonant inelastic x-ray scattering measurement on CH_3Cl. Sensitivity of K_α emission lines to nuclear dynamics through quenching of the vibrational broadening is observed. Furthermore, we performed polarization-resolved resonant inelastic x-ray-scattering measurements on CH_3Cl after resonant Cl K-shell excitation in order to probe the effects of molecular-field and singlet-triplet exchange effects on inner shells in neutral molecular species. We observe variation of the K_α spin-orbit doublet with the angle between emitted and incident polarization vectors. This dependence is explained as due to coupling between the chemical environment and singlet-triplet exchange. Although each individual $2p_{x,y,z}$ subcomponent of the spin-orbit doublets $2p_{3/2,\,1/2}$ cannot be resolved, we benefit from the polarization dependence, with the help of *ab initio* calculations, in obtaining sensitive determination of molecular populations within the spin-orbit doublet.

ACKNOWLEDGMENTS

These measurements were partially performed at the Swiss Light Source, Paul Scherrer Institute, Villigen, Switzerland. We gratefully acknowledge all the LUCIA beamline team at SLS: A.-M. Flanck, P. Lagarde, S. Bac, and D. Vantelon. We also thank the French Ministère de l'Education Nationale et de la Recherche - Programme *ACI-Jeunes Chercheurs (JC 4076)* for the financial support of this project. The authors thank the staff of the ALS for their excellent support. Support from the National Science Foundation (NSF) under Grant No. PHY-05-55699 is gratefully acknowledged. This work was partially performed at the Advanced Light Source, which is supported by (U.S.) Department of Energy (DOE) (DE-AC03-76SF00098).

[1] R. P. Wayne, *Chemistry of Atmospheres* (Oxford University Press, New York, 1991).
[2] R. A. Brownsword, M. Hillenkamp, T. Laurent, R. K. Vasta, and H.-R. Volpp, J. Phys. Chem. **101**, 5222 (1997).
[3] J. J. Lin, Y. chen, Y. T. Lee, and X. Yang, Chem. Phys. Lett. **361**, 374 (2002).
[4] G. Granucci, G. Medders, and A.-M. Velasco, Chem. Phys. Lett. **500**, 202 (2010).
[5] T. N. Olney, G. Cooper, W. F. Chan, G. R. Burton, C. E. Brion, and K. H. Tan, Chem. Phys. **205**, 421 (1996).
[6] S. Sundin, L. J. Saethre, S. L. Sorensen, A. Ausmees, and S. Svensson, J. Chem. Phys. **110**, 5806 (1999).
[7] D. L. Hansen, J. Cotter, G. R. Fisher, K. T. Leung, R. Martin, P. Neill, R. C.C. Perera, M. Simon, Y. Uehara, B. Vanderford, S. B. Whitfield, and D. W. Lindle, J. Phys. B **32**, 2629 (1999).
[8] R. Thissen, M. Simon, and M. J. Hubinfranskin, J. Chem. Phys. **101**, 7548–7553 (1994).
[9] C. Miron, P. Morin, D. Céolin, L. Journel, and M. Simon, J. Chem. Phys. **128**, 154314 (2008).

[10]D. Céolin, M. N. Piancastelli, R. Guilllemin, W. C. Stolte, S.-W. Yu, O. Hemmers, and D. W. Lindle, J. Chem. Phys. **126**, 084309 (2007).
[11]M. Kavčič, M. Žitnik, K. Bučar, M. Mihelič, M. Štuhec, J. Szlachetko, W. Cao, R. Alonso Mori, and P. Glatzel, Phys. Rev. Lett. **102**, 143001 (2009).
[12]P.-A. Raboud, M. Berset, J.-Cl. Dousse, Y.-P. Maillard, O. Mauron, J. Hoszowska, M. Polasik, and J. Rzadkiewicz, Phys. Rev. A **65**, 062503 (2002).
[13]M. Simon, L. Journel, R. Guillemin, W. C. Stolte, I. Minkov, F. Gel'mukhanov, P. Salek, H. Ågren, S. Carniato, R. Taïeb, A. C. Hudson, and D. W. Lindle, Phys. Rev. A **73**, 020706(R) (2006).
[14]M. Simon, L. Journel, R. Guillemin, W. C. Stolte, I. Minkov, F. Gel'mukhanov, P. Salek, H. Ågren, S. Carniato, R. Taïeb, A. C. Hudson, and D. W. Lindle, J. Electron Spectrosc. Relat. Phenom. **155**, 91 (2007).
[15]R. Guillemin, S. Carniato, W. C. Stolte, L. Journel, R. Taïeb, D. W. Lindle, and M. Simon, Phys. Rev. Lett. **101**, 133003 (2008).
[16]S. Carniato, R. Guillemin, W. C. Stolte, L. Journel, R. Taïeb, D. W. Lindle, and M. Simon, Phys. Rev. A **80**, 032513 (2009).
[17]S. Svensson, A. Ausmees, S. J. Osborne, G. Bray, F. Gel'mukhanov, H. Ågren, A. Naves de Brito, O.-P. Sairanen, A. Kivimäki, E. Nõmmiste, H. Aksela, and S. Aksela, Phys. Rev. Lett. **72**, 3021 (1994).
[18]H. Aksela, E. Kukk, S. Aksela, O.-P. Sairanen, A. Kivimäki, E. Nõmmiste, A. Ausmees, S. J. Osborne, and S. Svensson, J. Phys. B **28**, 4259 (1995).
[19]A. M. Bueno, A. N. de Brito, R. F. Fink, M. Bässler, O. Björneholm, F. Burmeister, R. Feifel, C. Miron, S. L. Sorensen, H. H. Wang, and S. Svensson, Phys. Rev. A **67**(2), 022714 (2003).
[20]L. Journel, L. El Khoury, T. Marin, R. Guillemin, S. Carniato, A. Avila, R. Delaunay, C. F. Hague, and M. Simon, Rev. Sci. Instrum. **80**, 093105 (2009).
[21]A.-M. Flank, G. Cauchon, P. Lagarde, S. Bac, M. Janousch, R. Wetter, J.-M. Dubuisson, M. Idir, F. Langlois, T. Moreno, and D. Vantelon, Nucl. Instrum. Methods Phys. Res. B **246**, 269 (2006).
[22]A. C. Hudson, W. C. Stolte, D. W. Lindle, and R. Guillemin, Rev. Sci. Instrum. **78**, 053101 (2007).
[23]S. Brennan, P. L. Cowan, R. D. Deslattes, A. Henins, D. W. Lindle, and B. A. Karlin, Rev. Sci. Instrum. **60**, 2243 (1989).
[24]P. Jensen, S. Brodersen, and G. Guelachvili, J. Mol. Spec. **88**, 378 (1981).
[25]T. R. Furlani and H. F. King, J. Chem. Phys. **82**, 5577 (1985).
[26]H. F. King and T. R. Furlani, J. Comput. Chem. **9**, 771 (1988).
[27]D. G. Fedorov and M. S. Gordon, J. Chem. Phys. **112**, 5611 (2000).
[28]M. W. Schmidt, K. K. Baldridge, J. A. Boatz, S. T. Elbert, M. S. Gordon, J. H. Jensen, S. Koseki, N. Matsunaga, K. A. Nguyen, S. Su, T. L. Windus, M. Dupuis, and J. A. Montgomery, Jr., J. Comput. Chem. **14**, 1347 (1993).
[29]T. Ziegler, A. Rauk, and E. J. Baerends, Theor. Chim. Acta **43**, 261 (1977).
[30]J. Javanainen, J. H. Eberly, and Q. Su, Phys. Rev. A **38**, 3430 (1988).
[31]D. E. Woon, T. H. Dunning,Jr., R. Seeger, and J. A. Pople, J. Chem. Phys. **98**, 1358 (1993).
[32]R. Krishnan, J. S. Binkley, R. Seeger, and J. A. Pople, J. Chem. Phys. **72**, 650 (1980).
[33]D. W. Lindle, P. L. Cowan, R. E. Lavilla, T. Jach, R. D. Deslattes, B. Karlin, J. A. Sheehy, T. J. Gil, and P. W. Langhoff, Phys. Rev. Lett. **60**, 1010 (1988).
[34]J. A. Campbell, At. Data Nucl. Data Tables **77**, 1451 (2001).
[35]M. O. Krause and J. H. Oliver, J. Phys. Chem. Ref. Data **8**, 329 (1979).
[36]M. Kavčič, M. Žitnik, K. Bučar, A. Mihelič, S. Carniato, L. Journel, R. Guillemin, and M. Simon, Phys. Rev. Lett. **105**, 113004 (2010).
[37]F. Gelmukhanov, P. Salek, T. Privalov, and H. Agren, Phys. Rev. A **59**, 380 (1999).
[38]F. Gelmukhanov and H. Agren, Phys. Rep. **312**, 87 (1999).
[39]T. Åberg and B. Crasemann, in *Resonant Anomalous X-Ray Scattering. Theory and Applications*, edited by G. Materlik, C. J. Sparks, and K. Fischer (North-Holland, Amsterdam, 1994), p. 431.
[40]F. Gelmukhanov and H. Ågren, Phys. Rev. A **49**, 4378 (1994).
[41]T. Marchenko, L. Journel, T. Marin, R. Guillemin, S. Carniato, M. Žitnik, M. Kavčič, K. Bučar, A. Mihelič, J. Hoszowska, W. Cao, and M. Simon, J. Chem. Phys. **134** 144308 (2011).
[42]D. W. Lindle, P. L. Cowan, T. Jach, R. E. Lavilla, and R. D. Deslattes, Phys. Rev. A **43**, 2353 (1991).
[43]M. A. MacDonald, S. H. Southworth, J. C. Levin, A. Henins, R. D. Deslattes, T. LeBrun, Y. Azuma, P. L. Cowan, and B. A. Karlin, Phys. Rev. A **51**, 3598 (1995).
[44]S. H. Southworth, D. W. Lindle, R. Mayer, and P. L. Cowan, Phys. Rev. Lett. **67**, 1098 (1991).
[45]Y. Luo, H. Ågren, and F. Gel'mukhanov, J. Phys. B **27**, 4169 (1994).